sustainability

MDPI

Article

Potential of Ripe Plantain Fruit Peels as an Ecofriendly Catalyst for Biodiesel Synthesis: Optimization by Artificial Neural Network Integrated with Genetic Algorithm

Anietie O. Etim [1], Eriola Betiku [1,*], Sheriff O. Ajala [1,2], Peter J. Olaniyi [3] and Tunde V. Ojumu [1,4]

1 Department of Chemical Engineering, Obafemi Awolowo University, Ile-Ife 220005, Osun State, Nigeria; etimanietie@yahoo.com (A.O.E.); sheriffajalao@gmail.com (S.O.A.); ojumut@cput.ac.za (T.V.O.)
2 Sustainable Energy Systems Engineering, Texas A&M University-Kingsville, Kingsville, TX 78363, USA
3 Department of Chemistry, Obafemi Awolowo University, Ile-Ife 220005, Osun State, Nigeria; saintlyscholar_pj@yahoo.com
4 Department of Chemical Engineering, Cape Peninsula University of Technology, Cape Town Campus, Keizersgracht and Tennant Street Zonnebloem, Cape Town 8000, South Africa
* Correspondence: ebetiku@oauife.edu.ng or ebetiku@yahoo.com; Tel.: +234-803-660-2988

Received: 27 December 2017; Accepted: 5 February 2018; Published: 6 March 2018

Abstract: The present work was aimed at assessing the possible use of ripe plantain fruit peel as a green-base catalyst in synthesizing *Azadirachta indica* oil methyl esters (AIOME). The free fatty acid content of the oil (5.81 wt %) was initially reduced to 0.90 wt % using methanol: oil at 2.19 v/v, $Fe_2(SO_4)_3$ at 6 wt %, time of 15 min and temperature of 65 °C. The pretreated oil was converted to AIOME in a transesterification process with calcined ripe plantain peel ash (CRPPA) at 700 °C as catalyst. The process was modeled by artificial neural network and optimized using genetic algorithm. The effectiveness of the developed CRPPA is ascribable to its high K content and microstructural transformation. The reliability of the model obtained was confirmed with a high coefficient of determination (R^2) of 0.996 and a low mean relative percentage deviation (MRPD) of 8.10%. The best operating variables combination for the process was methanol:oil of 0.73 v/v, CRPPA of 0.65 wt % and time of 57 min while the temperature was kept constant at 65 °C with a corresponding AIOME yield of 99.2 wt %. The results of this work demonstrated the potentials of ripe plantain peels and neem oil as cheap feedstocks for biodiesel production.

Keywords: artificial neural network; biodiesel; heterogeneous catalyst; modeling; optimization; transesterification

1. Introduction

Biodiesel production is now a topical issue and a subject which has been receiving huge attention worldwide for the past two decades. The reasons for this spike are well documented [1]. The prospect of biodiesel as a replacement for petro-diesel is largely due to its renewable nature, less pollutant emissions, miscibility with petro-diesel, and inherent lubricity [2]. However, studies have shown that the contest with respect to the issue of food versus fuel debate can be adequately addressed by employing the use of oils that are non-edible or wastes [3]. The current trends on biobased catalyst development has also shown that the higher cost of biodiesel over petro-diesel may be reduced using heterogeneous catalysts coupled with the advantages such as reusability and easily separable from biodiesel.

Previous studies have reported various improved yields of biodiesel using biobased catalysts which were calcined at varying temperatures. In addition, optimization tools have been employed to facilitate the predictions of operating and reaction parameters necessary to achieve optimum yield. Onoji et al. [4] reported the production of biodiesel using rubber seed oil, methanol, and calcined rubber seed kernel wastes at 800 °C and achieved 83.06% yield using response surface methodology (RSM). We recently demonstrated that by using cocoa pod husk ash calcined at 700 °C as the catalyst, 99.3 wt % biodiesel yield could be achieved using neem oil and methanol via the transesterification process, which was optimized using RSM [5]. In Tan et al. [6], waste cooking oil, methanol, and Ostrich-eggshell ash calcined at 1000 °C were used to attain 96 wt % biodiesel yield in a transesterification reaction carried out at room temperature while 96 wt % yield biodiesel was obtained from yellow oleander oil and methanol using burnt banana trunk as catalyst [7], however both studies were not optimized. In a separate study, both RSM and artificial neural network (ANN) were used to optimize the transesterification reaction of yellow oleander oil and methanol using unripe plantain peel ash calcined at 500 °C as catalyst. The study showed that 95% yield of biodiesel can be achieved in this process [8]; the study also showed that ANN was better than RSM in terms of accuracy and predictive capabilities. Table 1 shows a brief review of various base heterogeneous catalysts previously investigated together with the vegetable oils, conditions of transesterification, and biodiesel yields obtained.

Table 1. Comparison of heterogeneous catalysts for fatty acid methyl esters production via transesterification.

Heterogeneous Catalyst Type	Feedstock	Surface Area (m^2/g)	Catalyst Dosage (wt %)	Alcohol/Oil Ratio	Temperature (°C)	Time (min)	Yield (wt %)	Reference
Rubber seed shell	Rubber seed oil	352.51	2.2	0.2 [a]	60	60	83.11 [b]	[4]
Cocoa pod husks	Neem oil	2.76	0.65	0.73 [a]	65	57	99.3 [b]	[5]
Ostrich-egg shell	Waste cooking oil	71.00	1.5	12 [c]	65	120	96 [b]	[6]
Chicken-egg shell	Waste cooking oil	54.60	1.5	12 [c]	65	120	94 [b]	[6]
Unripe plantain peels	Yellow oleander oil	NR	2.8	0.3 [a]	60	75	94.97 [b]	[8]
Banana peels	Napoleon's plume oil	4.442	2.75	7.6 [c]	65	69.02	98.50 [b]	[9]
Banana peels	Waste cooking oil	14.036	2	6 [c]	60	180	100 [b]	[10]
Coconut husk	Jatropha oil	—	7	12 [c]	45	45	99.86 [d]	[11]
Torrey ash	Jatropha oil	9.622	5.0	9 [c]	65	300	89.43 [d]	[12]
River snail shells	Palm oil	3.495	5	12 [c]	65	90	98.50 [b]	[13]
Waste chicken bones	Waste cooking oil	98.54	5	15 [c]	65	240	89.33 [b]	[14]
Sea sand	Soybean oil	4.60	7.5	12 [c]	60	360	97.50 [d]	[15]
Pyrolyzed rice husk	Waste cooking oil	4.00	5	20 [c]	110	900	87.57 [b]	[16]
Coal fly ash-derived sodalite	Soy oil	10.00	4	12 [c]	65	120	95.50 [b]	[17]

[a]—volume ratio, [b]—production yield (wt%), [c]—molar ratio, [d]—methyl ester content (wt %).

It should be noted that ANN is a machine learning tool, which mimics the biological processing ability like the human brain. It can handle simulation of very complex and non-linear systems due to its capability to use learning algorithms and establish the relationship between input and output variables [18]. One key advantage of ANN is that it can be used to predict outputs of a new input data set once a data set has been trained well by a neural network. ANNs have been successfully applied as a modeling tool in many research areas, including esterification [19] and transesterification [8,20,21] processes. In the work of Betiku and Ajala [8] in which the efficacy of ANN was tested, the authors used calcined unripe plantain peel as a heterogeneous catalyst, yellow oleander oil and methanol for the transesterification reaction. Whereas, Avramovic et al. [20] applied ANN to the transesterification reaction in which synthetic CaO as a heterogeneous catalyst, sunflower oil and ethanol were used. While Sarve et al. [21] employed ANN in the ultrasound-assisted transesterification using barium hydroxide as a heterogeneous catalyst, sesame oil and methanol. In order to maximize or minimize the response of an objective function, models generated using ANN are usually coupled with an optimization tool such as genetic algorithm, GA [20,22], particle swarm

optimization, PSO [23], rotation inherit optimization, RIO [24], to achieve this by optimizing the operating input variables involved.

Plantain (*Musa paradisiacal*) is a common staple food in West Africa, which is consumed boiled, fried, roasted, or baked. Although people do eat unripe plantain in some countries, it is noteworthy that people generally prefer ripe ones. About half of the World's plantain production comes from West and Central Africa, and Nigeria is one of the leading producers [25]. In 2014, the World production was 30.7 million metric tons, of which Nigeria produced 3.04 million metric tons [25]. The high consumption of plantain fruits in Nigeria in particular and by extension in West Africa, produces solid wastes in the form of peels, which are typically discarded and only a small fraction of them are fed to goats locally.

Although we have previously shown the potential of unripe plantain fruit peel ash as catalyst for yellow oleander biodiesel production [8], it could be argued that catalyst development from the plantain may have a negative impact on food security from this source as it was earlier highlighted that plantain are generally consumed when ripened. Thus, this present work focused on the development of a catalyst from ripe plantain fruit peels with emphasis on the catalyst characterization which was hither to not reported in our previous study but may be a useful resource with respect to future development of this catalyst. The developed catalyst was used for production of biodiesel using *Azadirachta indica* (neem) oil. The transesterification process used for the biodiesel production was modeled using ANN. GA integrated with the developed model was used to establish the best operating input parameters for maximum biodiesel yield. The quality of the biodiesel produced was compared with standard specifications (ASTM D 6751 and DIN EN 14214).

2. Materials and Methods

2.1. Materials

Ripe plantain (*M. paradisiacal*) fruit peels used in this work were collected from restaurants within the Obafemi Awolowo University campus, Ile-Ife, Nigeria. The neem oil employed for this study was procured from the National Research Institute for Chemical Technology, Zaria, Kaduna State, Nigeria. All the chemicals and reagents used for this study were of analytical grades.

2.2. Catalyst Preparation from Ripe Plantain Peels

The ripe plantain peels collected were initially washed 3 times with distilled water and cut to small pieces after which they were oven-dried at 80 °C for 24 h. The dried pieces of peels were ground to powder using a porcelain pestle and mortar. A portion of the powder was ashed by open burning, part of which was calcined in a muffle furnace at varying temperature (500, 700, 900, and 1100 °C) for 4 h [5,9]. The calcined ripe plantain peel ash (CRPPA) samples produced were homogenized using a pestle and mortar and were stored in corked plastic vessels for further analysis. The rest of the ground (burnt and unburnt plantain) peel samples were stored for further analysis [5,9].

2.3. Characterization of Heterogeneous Catalyst

AURIGA high resolution SEM coupled with a CDU-lead detector at 5 kV with tungsten filament (Zeiss Germany) integrated with energy dispersive X-ray spectroscopy (EDS) was used to investigate the microstructural morphology and the elemental composition of the unburnt, burnt and CRPPA samples at the temperatures investigated [5,9]. The elemental compositions reported in this work are mean of three replicates determined at different locations on the sample microstructures from SEM [5]. The porosity and surface area of the CRPPA were determined via Brunauer-Emmett-Teller (BET) method of adsorption of nitrogen gas with the aid of Micromeritics instrument (ASAP 2020). While the total pore volume and the average pore size of the CRPPA were measured by the Barret-Joyner-Halenda (BJH) method. FT-IR spectrophotometer (Thermo-Nicolet iS10) coupled with attenuated total reflectance (ATR) was used to identify the active surface functional groups present in the raw plantain peel (RPP), open-air burnt RPP and CRPPA samples. The FT-IR spectra of the samples

were obtained in the wavelength range of 4000–400 cm^{-1} [5]. For amorphous and crystalline structures determination, XRD structures were obtain using a D8 Advance diffractometer (Bruker AXS, Karlsruhe, Germany) with Cu-Kα radiation ($\lambda K\alpha_1$ = 1.5406 Å) integrated with a detector (LynxEye PSD) [5].

2.4. Experimental Design for the Transesterification Process

The central composite design (CCD) of RSM was applied for the experimental design for the transesterification process. A three-factor-five-level fractional factorial design (Table 2) was used to generate 20 experimental conditions (Table 3) employed in investigating the effect of methanol:oil (0.23:1–1.07:1 *v*/*v*), catalyst loading (0.65–4.85 wt %) and time (24.77–75.23 min) on the yield of methyl esters using the pretreated neem oil. The CCD was composed of 6 axial points, 8 factorial points and 6 central points to provide information regarding the interior of the experimental region.

Table 2. Independent factors used for CCD in transesterification of neem oil.

Factor	Unit	Coded Factor Levels				
		$-\alpha$	−1	0	1	$+\alpha$
Methanol/oil ratio (X_1)	*v*/*v*	0.23	0.40	0.65	0.90	1.07
Catalyst loading (X_2)	wt %	0.65	1.50	2.75	4.00	4.85
Reaction time (X_3)	min	24.77	35	50	65	75.23

Table 3. CCD, observed, predicted and residual values for transesterification of neem oil.

Run	Methanol/Oil Ratio (*v*/*v*)	Catalyst Loading (wt %)	Reaction Time (min)	Observed AIOME (wt %)	Predicted AIOME (wt %)
1 *	0.65 (0)	0.65 ($-\alpha$)	50.00 (0)	97.00	97.00
2	0.65 (0)	2.75 (0)	50.00 (0)	98.50	98.55
3	0.40 (−1)	4.00 (1)	65.00 (1)	94.50	94.50
4	0.90 (1)	1.50 (−1)	65.00 (1)	98.80	98.80
5	0.23 ($-\alpha$)	2.75 (0)	50.00 (0)	85.50	85.50
6	0.65 (0)	4.85 ($+\alpha$)	50.00 (0)	97.00	97.00
7	0.65 (0)	2.75 (0)	50.00 (0)	98.30	98.55
8 *	0.90 (1)	4.00 (1)	35.00 (−1)	91.00	91.00
9	0.40 (−1)	4.00 (1)	35.00 (−1)	97.40	97.40
10	0.65 (0)	2.75 (0)	75.23 ($+\alpha$)	97.10	97.10
11	0.65 (0)	2.75 (0)	50.00 (0)	99.30	98.55
12	0.90 (1)	4.00 (1)	65.00 (1)	93.70	93.70
13	0.65 (0)	2.75 (0)	24.77 ($-\alpha$)	97.40	97.40
14	0.90 (1)	1.50 (−1)	35.00 (−1)	95.00	95.00
15 *	1.07 ($+\alpha$)	2.75 (0)	50.00 (0)	95.00	95.00
16	0.40 (−1)	1.50 (−1)	35.00 (−1)	97.80	97.80
17	0.65 (0)	2.75 (0)	50.00 (0)	98.40	98.55
18	0.65 (0)	2.75 (0)	50.00 (0)	98.60	98.55
19	0.40 (−1)	1.50	65.00 (1)	97.80	97.80
20	0.65 (0)	2.75	50.00 (0)	98.20	98.55

α = 1.682, asterisk (*) runs represent the testing set while without the asterisk are the training set.

2.5. Model Development and Optimization

The modeling of the transesterification process in this present study was executed using Neural Power CPC-X Software (version 2.5). AIOME yield prediction was investigated by evaluating the performance of both the multilayer full feedforward (MFFF) and multilayer normal feed forward (MNFF) neural networks. The neural networks were trained by incremental back propagation (IBP) learning algorithm. The architecture used consisted of an input layer with three neurons (methanol:oil, catalyst loading and time), an output layer with one neuron (AIOME yield), and a hidden layer. The sigmoid transfer function (Equation (1)) and pure-linear transfer function (Equation (2)) were selected for the hidden and output layers, respectively. Each neural network was trained using a default stopping criteria of 100,000 iterations [8,22]. Other parameters were chosen as the default values of the software. The number of hidden neurons was determined by testing several neural networks iteratively

until the root mean square error (RMSE) value of the output was minimized [8,22]. The experimental data set was divided into two subsets: training set and testing set [21].

$$\psi(x) = \frac{1}{1 + e^{-x}} \tag{1}$$

$$\psi(x) = x \tag{2}$$

The efficacy of the developed model was assessed by comparing predicted responses with experimental responses. To choose the best model, the coefficient of determination (R^2) and mean relative percentage deviation (MRPD) were determined using Equations (3) and (4), respectively:

$$R^2 = 1 - \sum_{i=1}^{n} \left(\frac{\left(x_{i,cal} - x_{i,exp}\right)^2}{\left(x_{avg,exp} - x_{i,exp}\right)^2} \right) \tag{3}$$

$$\text{MRPD } (\%) = \left(\frac{1}{n} \sum_{i=1}^{n} \left(\frac{x_{i,exp} - x_{i,cal}}{x_{i,exp}} \right) \right) \times 100 \tag{4}$$

where n is the number of experimental data, $x_{i,cal}$ is the predicted values, $x_{i,exp}$ is the experimental values, and $x_{avg,exp}$ is the average experimental values.

Optimization of the operating variables for the transesterification process was carried out using Neural Power CPC-X Software (version 2.5). The three operating variables that denote the inputs for the developed model, were optimized using the GA method. The developed model was coupled with GA and used to predict the optimal condition of the input variables for maximum AIOME yield. The predicted optimum values were validated by carrying out triplicate experiments using these values, and the average observed values obtained were compared with the predicted responses [22].

2.6. Biodiesel Synthesis via Two-Step Transesterification

Although a two-step transesterification process was adopted for the methyl esters synthesis, we previously showed that the acid value of the neem oil used in this study could be reduced from 5.81% to 0.90% in the first-step pretreatment process using methanol:oil of 2.19 v/v, $Fe_2(SO_4)_3$ of 6 wt %, reaction time of 15 min and temperature of 65 °C [5]. This step is critical to avoid the saponification reaction, which poses a separation problem [9]. For the second step (transesterification process), specific quantities of the pretreated neem oil and methanol were measured into a 250-mL three-necked glass reactor connected to a reflux system and were allowed to mix for 5 min [9]. Further, a specific quantity of the CRPPA was added into the mixture in the glass reactor and the reaction was carried out for a specific period of time as stipulated in the design matrix (Table 3) at temperature of 65 °C [26–28]. After separation of the mixture at the end of the reaction, the AIOME produced was washed three times with warm distilled water at 50 °C to remove residuals [9]. The washed AIOME was further dried using sodium sulfate. The biodiesel yield was determined by Equation (5).

$$\text{AIOME yield } (\text{wt}\%) = \frac{\text{Weight of AIOME produced}}{\text{Weight of pretreated oil used}} \times 100 \tag{5}$$

2.7. Characterization of AIOME

The physical, chemical and fuel properties of the AIOME produced were determined as previously described by Betiku et al. [22]. The fuel properties such as flash point, pour point, and cloud point were determined via ASTM D 93, ASTM D 97, and ASTM D 2500, respectively. The fatty acid profile of the AIOME was analyzed by gas chromatography as described in our earlier studies [22]. To investigate possible leaching of group I metals (Na, K) and group II metals (Ca, Mg) from the CRPPA into the biodiesel during synthesis, the concentrations of the metallic elements in both washed and unwashed biodiesel products were determined using atomic adsorption spectrophotometry [5].

3. Results and Discussion

3.1. CRPPA Characterization

Table 4 shows the results of the EDS analysis carried out between 500 and 1100 °C. The results demonstrated that the calcination temperature significantly affected the elemental composition of the CRPPA. The major elements present in the CRPPA samples were O, Mg, P, S, K, Si, and Cl. Except for 900 °C, K had the highest mass fraction irrespective of the calcination temperature applied, but its highest mass fraction was observed at 700 °C (Table 4). Thus, the mass production of the ash was carried out at 700 °C and this was used afterwards as catalyst for the biodiesel synthesis. One can therefore speculate that K was the chief active element responsible for the catalytic action of the CRPPA in the AIOME synthesis.

Table 4. Elemental composition of CRPPA.

Temperature	O	Mg	P	S	K	Ca	Si	Cl	Al
(°C)	(wt %)								
500	38.99	0.80	1.23	0.00	43.49	0.00	7.41	8.09	0.00
700	36.43	1.15	1.84	0.47	51.02	0.00	2.51	6.27	0.29
900	45.81	0.55	2.80	0.66	39.20	3.23	5.56	1.46	0.00
1100	40.91	0.41	5.38	1.39	47.38	0.00	1.78	2.29	0.46

It has been shown that K has the highest concentration of all metals present in calcined cocoa pod husk [5], banana fruit peel [9,29], and unripe plantain fruit peel [8,29,30]. K was revealed to have the highest mass fraction in cocoa pod husk [5], ripe banana fruit peel [9], and unripe plantain fruit peel [8] when calcined at 500 °C for 4 h, 700 °C for 4 h, and 500 °C for 3.5 h, respectively.

Figure 1a–c displays the SEM images taken at a magnification of 1000× for raw, open air, and calcined ripe plantain peel samples. The surface transformation of the catalyst can be seen from the smooth and flatness nature of the raw plantain peel sample (Figure 1a) to a mix of smaller aggregates and flat surfaces obtained from the open-air burnt catalyst (Figure 1b) and a spongy and fibrous microstructure resulting from calcination at 700 °C for 4 h. The resulting microstructure is indicative of the increased surface area of the catalyst due to calcination, which may increase its catalytic activity.

It should be noted that thermal treatment via calcination prevents leaching of K thereby increasing the reusability of the catalyst [31].

The pore size, pore volume, and surface area of the CRPPA were measured. The adsorption average pore width (4 V/A by BET) was determined as 68.35 Å. The single point adsorption total pore volume of pores less than 2573.24 Å diameter at p/p° = 0.992508 was measured as 0.032122 cm^3/g. The BJH adsorption cumulative volume pores between 17.00 and 3000.00 Å was 15.20 m^3/g, while the BJH desorption cumulative volume pores between 17.00 and 3000.00 Å was 15.73 m^3/g. The BET surface area and t-plot external surface area of the CRPPA were 18.80 and 26.54 m^2/g, respectively.

The functional groups present in the RPP, open-air burnt RPP and CRPPA (at 700 °C) were determined by FT-IR analysis and the spectrum for each sample is depicted in Figure 2. All the spectra show various adsorption peaks. The peaks detected at 3300 to 3100 cm^{-1} in RPP and open-air burnt RPP samples (Figure 2) are ascribed to bending and stretching vibration of O–H bonds due to the existence of water molecules [32]. The peaks are however not detected in the CRPPA expectedly due to the heat treatment at 700 °C. While the peaks at 2920 and 2850 cm^{-1} found in the RPP sample are allocated strong asymmetric stretching vibration of $–CH_2$ and strong symmetric stretching vibration of $–CH_2$, respectively [33]. Observed peaks at 1600, 1396 and 1150 cm^{-1} in all the samples are assigned to carbonate C–O stretching and bending vibrations [9], which is an indication of the presence of carbonate. The peak at 1396 cm^{-1} is very strong in both open-air burnt RPP and CRPPA (Figure 2) and it is known for K_2CO_3 [9,31,34,35]. Furthermore, the peaks located at 1005 cm^{-1} is ascribed to Si–O–Si asymmetric stretching vibration [34,36]. The peak at 890 cm^{-1} observed in both open-air burnt RPP

and CRPPA may be due to an isolated SiO_4 vibration in $CaMgSiO_4$ agitated by contact with Ca^{2+} and Mg^{2+} [37].

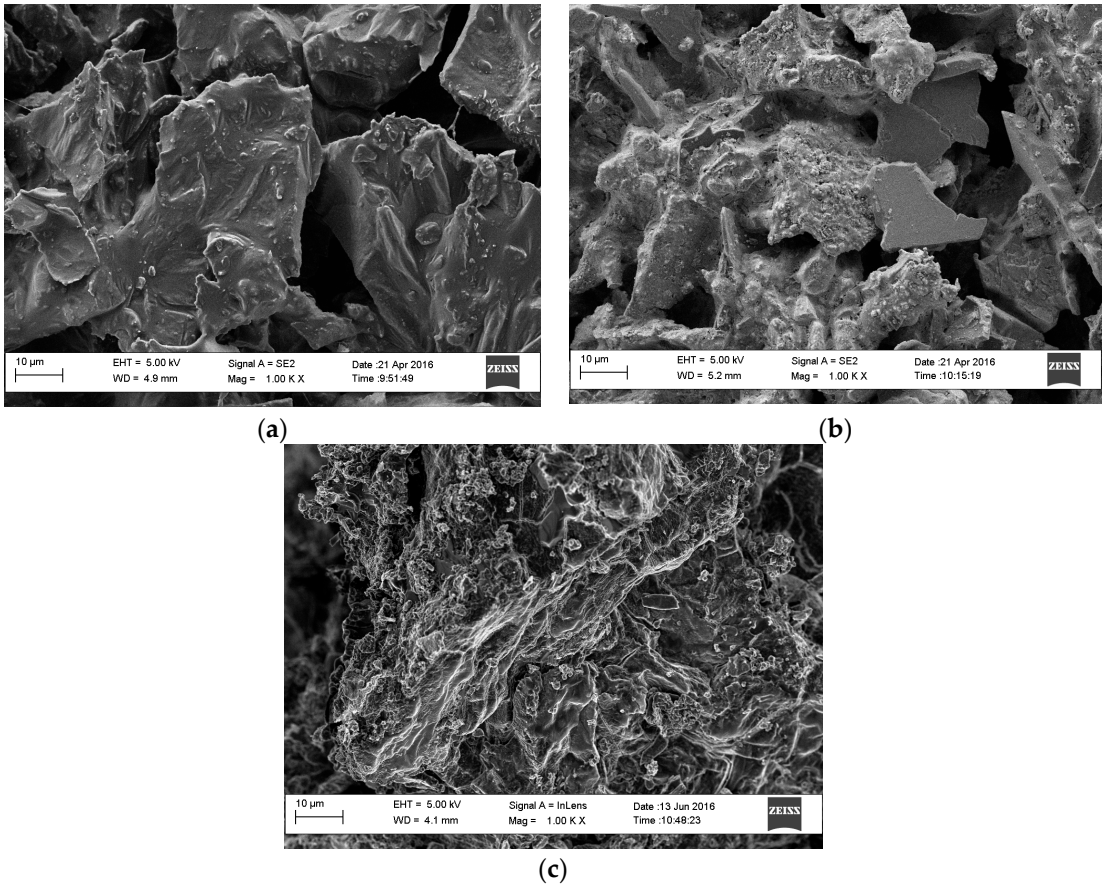

Figure 1. SEM images of (**a**) raw, (**b**) open-air burnt RPP and (**c**) CRPPA at 700 °C samples.

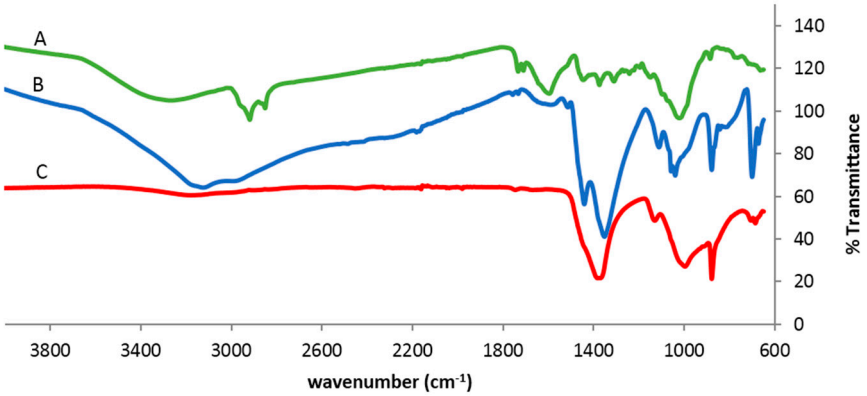

Figure 2. FT-IR spectra of (**A**) raw, (**B**) open-air burnt RPP and (**C**) CRPPA at 700 °C samples.

XRD diffraction was carried out to identify the crystalline compounds in the raw, open-air burnt, and calcined RPP samples (Figure 3). As heat treatment of the RPP increased, potassium compounds steadily increased (Figure 3). This trend has been reported in calcined catalytic biomass materials in previous studies [5].

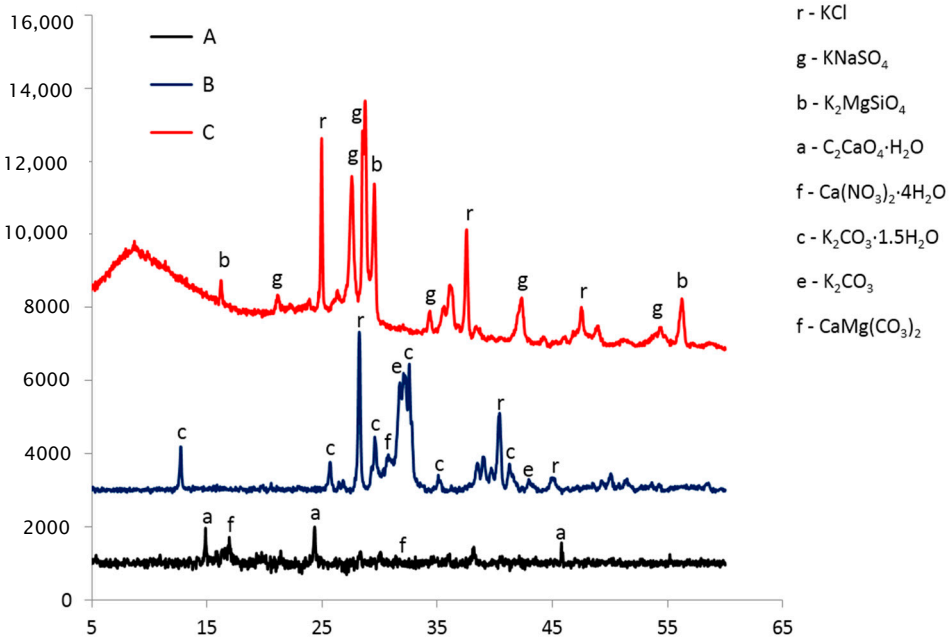

Figure 3. XRD chromatograms of (**A**) raw, (**B**) open-air burnt RPP and (**C**) CRPPA at 700 °C samples.

3.2. AIOME Synthesis Using CRPPA

3.2.1. Parameters Optimization for AIOME Synthesis

Various neural network architectures and topologies were developed and tested for prediction of AIOME yield and the network predictive capabilities were evaluated using R^2 and MRPD [8,22]. The results show that out of the six models developed (Table 5), the IBP with sigmoid and linear transfer functions as hidden and output layers, respectively, was the most efficient algorithm for AIOME yield prediction (Table 5). A series of network topologies were examined by varying the number of neurons from 2–8 to determine the optimum number of neurons in the hidden layer (Figure 4). The best topology (3-4-1), which has three inputs, four neurons as the optimum and one output, was selected because the R^2 for the testing, training, and whole data sets were the highest, while their MRPD values were the least of all the topologies (Table 5). The network mode developed for the chosen model is shown in Figure 5. The R^2 and MRPD for the training set were 0.996 and 9.57%, respectively while in the case of testing set, the values were unity and 0.0006%, respectively. The regression plot of the predicted AIOME yield values against the experimental AIOME yield values (Figure 6) supported the high value of R^2 and low value of MRPD. These results imply that the empirical model derived from ANN can be used adequately to describe the relationship between the input variables and the AIOME yield.

Table 5. Effect of different neural network architecture and topologies for AIOME synthesis.

Name	Model	Learning Algorithm	Connection Type	Transfer Function Hidden Layer	Transfer Function Output Layer	R^2 Whole Data	MRPD Whole Data (%)
H55	3-4-1	IBP [a]	MFFF [b]	Sigmoid	Linear	0.9962	8.10
H54	3-4-1	IBP	MNFF [c]	Sigmoid	Linear	0.9962	8.10
G33	3-3-1	IBP	MNFF	Sigmoid	Linear	0.9546	46.82
G45	3-2-1	IBP	MFFF	Sigmoid	Linear	0.9220	71.76

[a] IBP—incremental back propagation; [b] MFFF—multilayer full feedforward; [c] MNFF—multilayer normal feedforward.

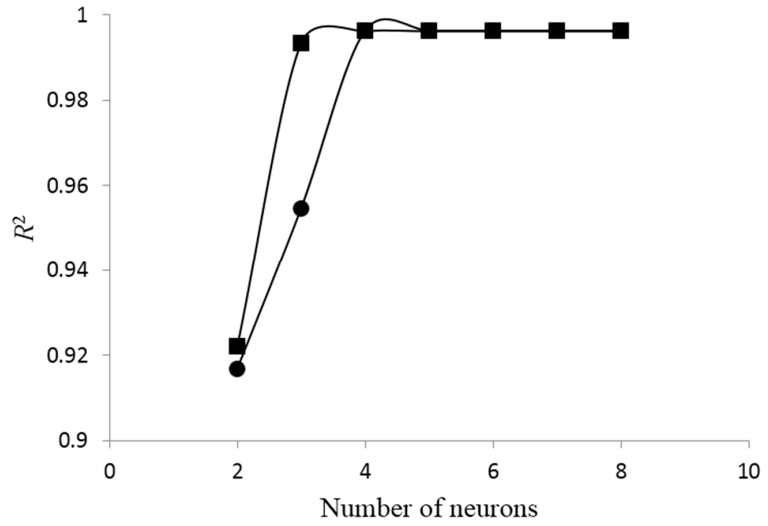

Figure 4. Optimum number of hidden neurons.

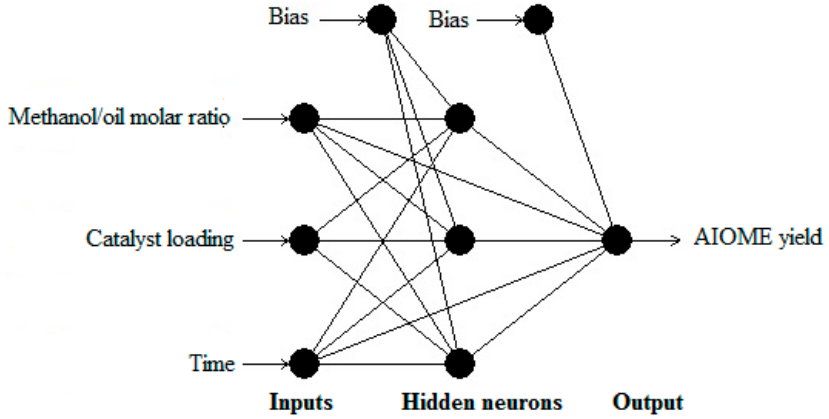

Figure 5. Neural network architecture.

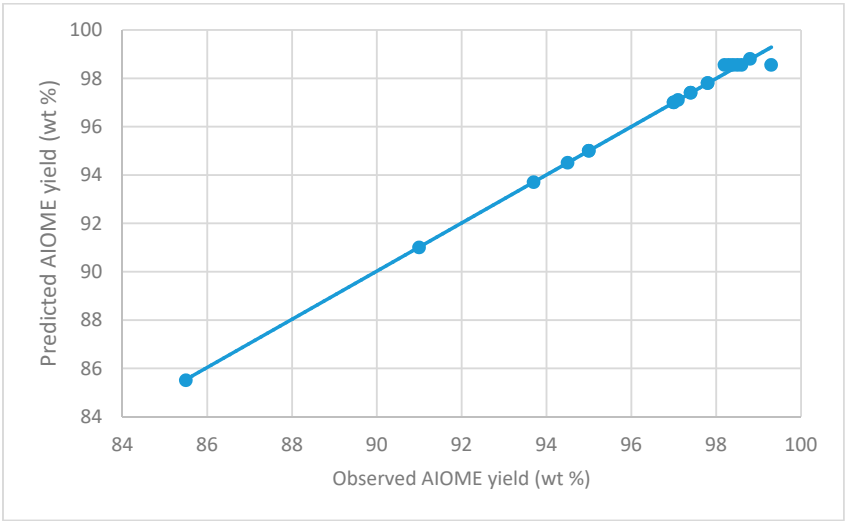

Figure 6. Parity plot of predicted values against observed values.

The optimal condition established for AIOME synthesis by integrating the developed model with GA was methanol:oil of 0.75 v/v, catalyst amount of 0.65 wt % and reaction time of 57 min,

while keeping the reaction temperature constant at 65 °C with a corresponding predicted AIOME yield of 99.2 wt %. Validation of the prediction was carried out by applying the optimum values to three independent experimental replicates and the average value of AIOME yield obtained was 99.3 wt %. These results confirmed the efficacy of the model developed.

Some agricultural wastes have been successfully applied as catalysts for biodiesel synthesis. For example, calcined banana fruits peel ash was used for Napoleon's plume (*Bauhinia monandra*) oil biodiesel production [9]. It was reported that an optimum biodiesel yield of 98.5 ± 0.18 wt % could be obtained using catalyst loading of 2.75 wt %, methanol:oil molar ratio of 7.6:1, reaction time of 69.02 min and reaction temperature constant at 65 °C. Biodiesel was produced using yellow oleander oil and unripe plantain fruit peel ash as catalyst by Betiku and Ajala [8]. The transesterification process was modeled and optimized by ANN-GA. The optimal condition was established as methanol:oil 0.3 v/v, reaction time 1.25 h, catalyst amount 2.8 wt % and reaction temperature of 60 °C with biodiesel yield of 95.09 wt %. Likewise, in our previous studies, neem oil and calcined cocoa pod husk ash were used to synthesize biodiesel [5]. RSM was used to establish the best operating variables combination for maximum biodiesel yield, which was reported as methanol:oil of 0.73 v/v, catalyst amount of 0.65 wt %, reaction time of 57 min and reaction temperature of 65 °C with an optimum yield of 99.3 wt %. Rubber seed oil and calcined rubber seed shell were both used to produce biodiesel [4]. The authors established the optimal condition using RSM as methanol:oil of 0.20 v/v, catalyst loading of 2.2 g/g, time of 60 min and reaction temperature of 60 °C with an optimum yield of 83.11 wt %.

3.2.2. Interactions of Independent Variables

The interactive effects of the input variables on the AIOME yield were investigated graphically (Figure 7). Figure 7a represents the three-dimensional plots of reaction time and methanol:oil on the AIOME yield while keeping the reaction temperature constant.

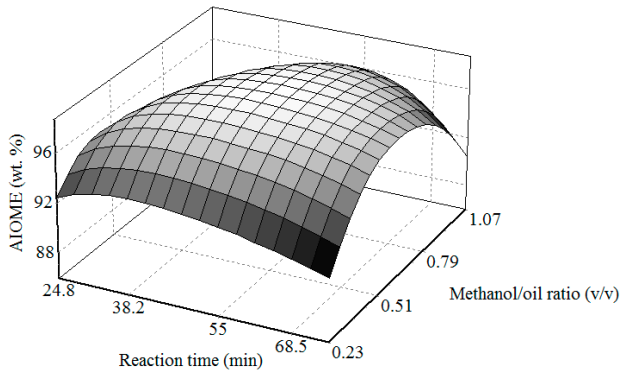

(**a**)

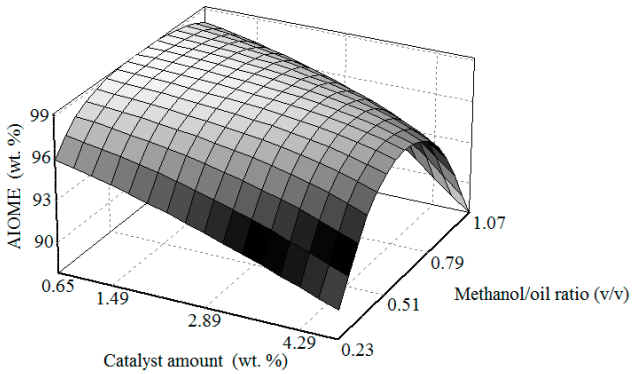

(**b**)

Figure 7. *Cont.*

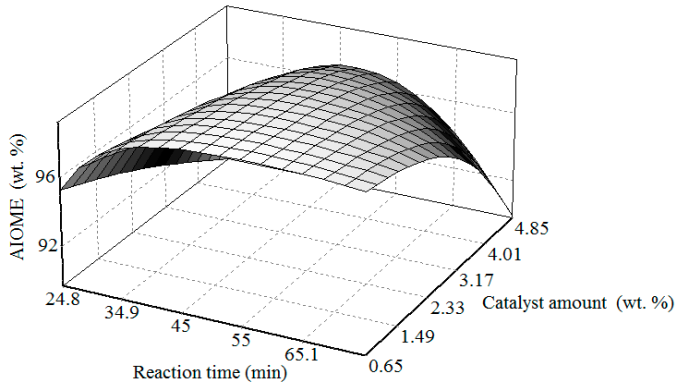

(**c**)

Figure 7. Surface plots of AIOME yield against (**a**) reaction time and methanol:oil; (**b**) catalyst amount and methanol:oil; (**c**) reaction time and catalyst amount.

The plots show that both methanol:oil and reaction time had a significant effect on the biodiesel yield. There appears to be an optimum for both variables about 55 min and 0.79 v/v (Figure 7a), which are close to the optimum predicted values. The three-dimensional plot of catalyst amount and methanol:oil against biodiesel yield while keeping the reaction temperature constant is depicted in Figure 7b. The significant influence of catalyst amount and methanol:oil on the AIOME yield is apparent from this plot. The interaction of reaction time and catalyst amount on biodiesel yield, while keeping the reaction temperature constant, is displayed in Figure 7c, which shows a significant interaction between the two variables.

The plots reveal high yield of AIOME can be obtained from reaction time range of 55–65 min and catalyst amount of 0.65 wt %. The curvature nature of the three-dimensional surfaces suggest significant interactions of methanol:oil, reaction time, and catalyst amount. Methanol:oil, reaction time and catalyst amount have been reported to have a strong effect on biodiesel yield [24,38,39]. Although in the transesterification reaction of oil and methanol, alcohol in excess of the required stoichiometric amount is needed to shift the equilibrium/reversible reaction towards biodiesel formation [38], its oversupply in the process may lead to dilution, which may reduce the biodiesel yield. Also, sufficient reaction time is needed to allow for adequate reactants interaction to form the product [24,38,39]. The time range selected for this work seems sufficient to obtain maximum AIOME yield.

The importance level of the three variables considered for the transesterification process were evaluated using Neural Power CPC-X Software (version 2.5) and the results shown in Figure 8. Methanol:oil with 54.44% was the most important variable, followed by catalyst amount with 26.47% and then reaction time with 19.09%.

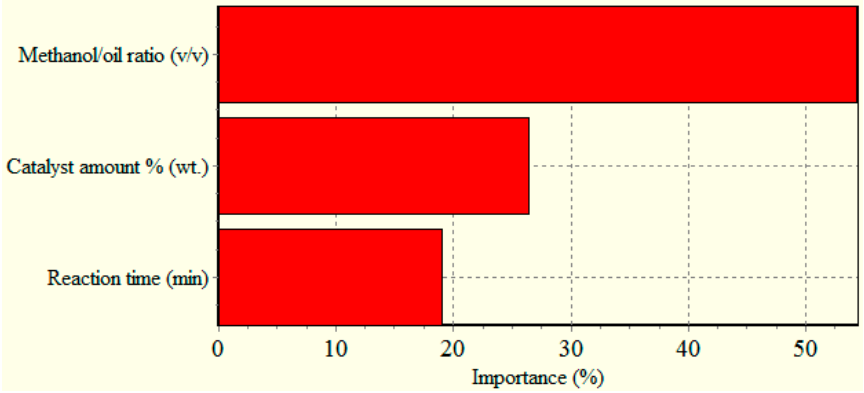

Figure 8. Level of importance of process variables in the transesterification reaction.

3.3. AIOME Quality Characterization and Its Fatty Acid Composition

The fuel properties of the AIOME produced using CRPPA were determined and the results are summarized in Table 6. The properties of the biodiesel produced compared very well with EN 14214 and ASTM D 6751 standard specifications. Also, these properties were similar to those earlier reported for neem oil biodiesel using calcined cocoa pod husk ash [5]. For example, the kinematic viscosity of 5.0 mm^2/s and acid value of 0.45 mg KOH/g oil for the biodiesel were within the limit specified by the standards. The kinematic viscosity of neem oil biodiesel earlier reported were 4.0 [24,40], 5.3 [5], and 5.5 mm^2/s [24,40], while the acid values earlier reported were 0.22 mg KOH/g oil [24,40] and 0.5 mg KOH/g oil [5].

Table 6. Properties of AIOME in comparison with biodiesel specification standards.

Parameter	Mean Value	ASTM D6751	EN 14214
Moisture content (%)	0.01	<0.03	0.02
Specific gravity	0.88	0.86–0.90	0.85
Kinematic viscosity (mm^2/s) at 40 °C	5.0	1.9–6.0	3.5–5.0
Acid value (mg KOH/g oil)	0.45	0.5 max	0.5 max
Iodine value (g I_2/100 g oil)	58.6	NS	120 max
Higher heating value (MJ/kg)	48.7	NS	NS
Cetane number	81	47 min	51 min
Group I metals (Na + K) (ppm)	1.80	5.0 max	5.0 max
Group II metals (Ca + Mg) (ppm)	0.42	5.0 max	5.0 max
Pour point (°C)	9	NS	NS
Cloud point (°C)	21	NS	NS
Flash point (°C)	274	130 min	101 min

NS = not specified.

The high value of the flash point (274 °C) for the AIOME indicates that it is safe to handle and store [41]. The feasibility of the CRPPA as a catalyst for biodiesel production was investigated by conducting a leaching test on the AIOME. The metallic elements analyzed in the washed AIOME include Na, K, Ca, and Mg. The washed AIOME had Na + K concentration of 1.8 ppm and Ca + Mg concentration of 0.42 ppm, while the unwashed AIOME had Na + K concentration of 115.6 ppm and Ca + Mg concentration of 0.96 ppm. The observed values of the washed sample satisfied the ASTM D 6751 standard specification (Table 6), which is an indication that the purification method employed in this work is effective in removing metallic elements that may have leached into the biodiesel. The fatty acid profile of the AIOME is presented in Table 7. The results showed that the biodiesel was highly unsaturated (73.79%) with linoleic acid, oleic acid, palmitic acid, and stearic acid as the major methyl esters. Earlier reports have revealed that methyl esters from neem oil are highly unsaturated [5,40].

Table 7. Fatty acid profile of AIOME.

Fatty Acid	Structure	% Composition
Saturated fatty acid		
Palmitic	C16:0	14.25
Stearic	C18:0	10.85
Arachidic	C20:0	0.57
Lignoceric	C24:0	0.55
Total		26.22
Unsaturated fatty acid		
Palmitoleic	C16:1	0.05
Oleic	C18:1	14.34
Linoleic	C18:2	59.10
Linolenic	C18:3	0.30
Total		73.79

4. Conclusions

Biodiesel synthesis was carried out using neem oil, methanol, and calcined plantain fruit peel ash in a 2-step transesterification process. The neem oil with a high free fatty acid content was first reduced to 0.90 wt % in an esterification reaction via methanol:oil of 2.19 v/v, $Fe_2(SO_4)_3$ of 6 wt %, reaction time of 15 min, and temperature of 65 °C. In the second step, ANN was used to model the transesterification process, while the operating variables in the process were optimized using GA for maximum biodiesel yield. The best algorithm for the AIOME yield prediction was IBP with sigmoid and linear transfer functions as hidden and output layers, respectively. The characterization of the CRPPA developed by XRD, FT-IR, and SEM-EDS showed that its catalytic activities may be due to its high K content and the microstructural alteration. The model developed has very high prediction accuracy and reliability with R^2 of 0.996 and MRPD of 8.10%. AIOME yield of 99.2 wt % could be obtained using a transesterification process operating variables combination of methanol:oil of 0.73 v/v, CRPPA of 0.65 wt % and reaction time of 57 min while maintaining the reaction temperature constant at 65 °C. The results of this work demonstrated that methanol:oil was the most important operating variable for the process and the biodiesel produced satisfied both the EN 14214 and ASTM D 6751 standard specifications. Although the potential of unripe plantain peels as catalyst for biodiesel production has been reported, the project highlights the prospect of ripe plantain peels and neem oil as feedstock for biodiesel production, thus removing the threat to food security which may arise due to the utilization of unripe plantain.

Acknowledgments: E.B. thankfully acknowledges the equipment donation from the World University Service, Wiesbaden, Germany. TVO acknowledges the financial support of the Cape Peninsula University of Technology (CPUT) for the catalyst development aspect of this project.

Author Contributions: E.B. conceived and designed the experiments; A.O.E. performed the experiments; and A.O.E., P.J.O. and T.V.O. developed the catalyst, E.B., A.O.E. and S.O.A. analyzed the data, A.O.E., E.B. and T.V.O. wrote the paper.

Conflicts of Interest: The authors declare no conflict of interest.

Abbreviations

AIOME	Azadirachta indica oil methyl esters
ANN	artificial neural network
ANOVA	analysis of variance
BET	Brunauer-Emmett-Teller
BJH	Barret-Joyner-Halenda
CCD	central composite design
CRPPA	calcined ripe plantain peel ash
FT-IR	Fourier transform infra-red
GA	genetic algorithm
IBP	incremental back propagation
MFFF	multilayer full feedforward
MNFF	multilayer normal feed forward
MRPD	mean relative percentage deviation
RPP	raw ripe plantain peel
R^2	coefficient of determination
RSM	response surface methodology
SEM	scanning electron microscope
XRD	X-ray diffraction

References

1. Knothe, G. "Designer" biodiesel: Optimizing fatty ester composition to improve fuel properties†. *Energy Fuels* **2008**, *22*, 1358–1364. [CrossRef]
2. Knothe, G. Biodiesel derived from a model oil enriched in palmitoleic acid, macadamia nut oil. *Energy Fuels* **2010**, *24*, 2098–2103. [CrossRef]

3. Leung, D.Y.; Wu, X.; Leung, M. A review on biodiesel production using catalyzed transesterification. *Appl. Energy* **2010**, *87*, 1083–1095. [CrossRef]
4. Onoji, S.E.; Iyuke, S.E.; Igbafe, A.I.; Daramola, M.O. Transesterification of rubber seed oil to biodiesel over a calcined waste rubber seed shell catalyst: Modeling and optimization of process variables. *Energy Fuels* **2017**, *31*, 6109–6119. [CrossRef]
5. Betiku, E.; Etim, A.O.; Pereao, O.; Ojumu, T.V. Two-step conversion of neem (*Azadirachta indica*) seed oil into fatty methyl esters using a heterogeneous biomass-based catalyst: An example of cocoa pod husk. *Energy Fuels* **2017**, *31*, 6182–6193. [CrossRef]
6. Tan, Y.H.; Abdullah, M.O.; Nolasco-Hipolito, C.; Taufiq-Yap, Y.H. Waste ostrich-and chicken-eggshells as heterogeneous base catalyst for biodiesel production from used cooking oil: Catalyst characterization and biodiesel yield performance. *Appl. Energy* **2015**, *160*, 58–70. [CrossRef]
7. Deka, D.C.; Basumatary, S. High quality biodiesel from yellow oleander (*Thevetia peruviana*) seed oil. *Biomass Bioenergy* **2011**, *35*, 1797–1803. [CrossRef]
8. Betiku, E.; Ajala, S.O. Modeling and optimization of *Thevetia peruviana* (yellow oleander) oil biodiesel synthesis via *Musa paradisiacal* (plantain) peels as heterogeneous base catalyst: A case of artificial neural network vs. response surface methodology. *Ind. Crops Prod.* **2014**, *53*, 314–322. [CrossRef]
9. Betiku, E.; Akintunde, A.M.; Ojumu, T.V. Banana peels as a biobase catalyst for fatty acid methyl esters production using napoleon's plume (*Bauhinia monandra*) seed oil: A process parameters optimization study. *Energy* **2016**, *103*, 797–806. [CrossRef]
10. Gohain, M.; Devi, A.; Deka, D. *Musa balbisiana* colla peel as highly effective renewable heterogeneous base catalyst for biodiesel production. *Ind. Crops Prod.* **2017**, *109*, 8–18. [CrossRef]
11. Vadery, V.; Narayanan, B.N.; Ramakrishnan, R.M.; Cherikkallinmel, S.K.; Sugunan, S.; Narayanan, D.P.; Sasidharan, S. Room temperature production of jatropha biodiesel over coconut husk ash. *Energy* **2014**, *70*, 588–594. [CrossRef]
12. Chouhan, A.P.S.; Sarma, A.K. Biodiesel production from *Jatropha curcas* L. oil using *Lemna perpusilla* Torrey ash as heterogeneous catalyst. *Biomass Bioenergy* **2013**, *55*, 386–389. [CrossRef]
13. Roschat, W.; Siritanon, T.; Kaewpuang, T.; Yoosuk, B.; Promarak, V. Economical and green biodiesel production process using river snail shells-derived heterogeneous catalyst and co-solvent method. *Bioresour. Technol.* **2016**, *209*, 343–350. [CrossRef] [PubMed]
14. Farooq, M.; Ramli, A.; Naeem, A. Biodiesel production from low FFA waste cooking oil using heterogeneous catalyst derived from chicken bones. *Renew. Energy* **2015**, *76*, 362–368. [CrossRef]
15. Muciño, G.G.; Romero, R.; Ramírez, A.; Martínez, S.L.; Baeza-Jiménez, R.; Natividad, R. Biodiesel production from used cooking oil and sea sand as heterogeneous catalyst. *Fuel* **2014**, *138*, 143–148. [CrossRef]
16. Li, M.; Zheng, Y.; Chen, Y.; Zhu, X. Biodiesel production from waste cooking oil using a heterogeneous catalyst from pyrolyzed rice husk. *Bioresour. Technol.* **2014**, *154*, 345–348. [CrossRef] [PubMed]
17. Manique, M.C.; Lacerda, L.V.; Alves, A.K.; Bergmann, C.P. Biodiesel production using coal fly ash-derived sodalite as a heterogeneous catalyst. *Fuel* **2017**, *190*, 268–273. [CrossRef]
18. Zobel, C.W.; Cook, D.F. Evaluation of neural network variable influence measures for process control. *Eng. Appl. Artif. Intel.* **2011**, *24*, 803–812. [CrossRef]
19. Rajendra, M.; Jena, P.C.; Raheman, H. Prediction of optimized pretreatment process parameters for biodiesel production using ANN and GA. *Fuel* **2009**, *88*, 868–875. [CrossRef]
20. Avramović, J.M.; Veličković, A.V.; Stamenković, O.S.; Rajković, K.M.; Milić, P.S.; Veljković, V.B. Optimization of sunflower oil ethanolysis catalyzed by calcium oxide: RSM versus ANN-GA. *Energy Convers. Manag.* **2015**, *105*, 1149–1156. [CrossRef]
21. Sarve, A.; Sonawane, S.S.;'Varma, M.N. Ultrasound assisted biodiesel production from sesame (*Sesamum indicum* L.) oil using barium hydroxide as a heterogeneous catalyst: Comparative assessment of prediction abilities between response surface methodology (RSM) and artificial neural network (ANN). *Ultrason. Sonochem.* **2015**, *26*, 218–228. [CrossRef] [PubMed]
22. Betiku, E.; Okunsolawo, S.S.; Ajala, S.O.; Odedele, O.S. Performance evaluation of artificial neural network coupled with generic algorithm and response surface methodology in modeling and optimization of biodiesel production process parameters from shea tree (*Vitellaria paradoxa*) nut butter. *Renew. Energy* **2015**, *76*, 408–417. [CrossRef]

23. Ghaedi, M.; Ansari, A.; Bahari, F.; Ghaedi, A.; Vafaei, A. A hybrid artificial neural network and particle swarm optimization for prediction of removal of hazardous dye brilliant green from aqueous solution using zinc sulfide nanoparticle loaded on activated carbon. *Spectrochim. Acta Part A Mol. Biomol. Spectrosc.* **2015**, *137*, 1004–1015. [CrossRef] [PubMed]
24. Betiku, E.; Omilakin, O.R.; Ajala, S.O.; Okeleye, A.A.; Taiwo, A.E.; Solomon, B.O. Mathematical modeling and process parameters optimization studies by artificial neural network and response surface methodology: A case of non-edible neem (*Azadirachta indica*) seed oil biodiesel synthesis. *Energy* **2014**, *72*, 266–273. [CrossRef]
25. FAOSTAT. Statistical Databases. Food and Agriculture Organization of the United Nations. Statistics Division. 2014. Available online: www.fao.org/faostat/en/#data/QC (accessed on 14 May 2017).
26. Zhang, J.; Chen, S.; Yang, R.; Yan, Y. Biodiesel production from vegetable oil using heterogenous acid and alkali catalyst. *Fuel* **2010**, *89*, 2939–2944. [CrossRef]
27. Olutoye, M.; Lee, S.; Hameed, B. Synthesis of fatty acid methyl ester from palm oil (*Elaeis guineensis*) with $k_y(MgCa)_{2x}O_3$ as heterogeneous catalyst. *Bioresour. Technol.* **2011**, *102*, 10777–10783. [CrossRef] [PubMed]
28. Naik, M.; Meher, L.; Naik, S.; Das, L. Production of biodiesel from high free fatty acid karanja (*Pongamia pinnata*) oil. *Biomass Bioenergy* **2008**, *32*, 354–357. [CrossRef]
29. Olabanji, I.O.; Oluyemi, E.A.; Ajayi, O.S. Metal analyses of ash derived alkalis from banana and plantain peels (Musa spp.) in soap making. *Afr. J. Biotechnol.* **2012**, *11*, 16512–16518.
30. Onyegbado, C.; Iyagba, E.; Offor, O. Solid soap production using plantain peel ash as source of alkali. *J. Appl. Sci. Environ. Manag.* **2002**, *6*, 73–77. [CrossRef]
31. Sharma, M.; Khan, A.A.; Puri, S.; Tuli, D. Wood ash as a potential heterogeneous catalyst for biodiesel synthesis. *Biomass Bioenergy* **2012**, *41*, 94–106. [CrossRef]
32. Nisar, J.; Razaq, R.; Farooq, M.; Iqbal, M.; Khan, R.A.; Sayed, M.; Shah, A.; Ur Rahman, I. Enhanced biodiesel production from jatropha oil using calcined waste animal bones as catalyst. *Renew. Energy* **2017**, *101*, 111–119. [CrossRef]
33. Qiu, F.; Li, Y.; Yang, D.; Li, X.; Sun, P. Biodiesel production from mixed soybean oil and rapeseed oil. *Appl. Energy* **2011**, *88*, 2050–2055. [CrossRef]
34. Lukić, I.; Krstić, J.; Jovanović, D.; Skala, D. Alumina/silica supported K_2CO_3 as a catalyst for biodiesel synthesis from sunflower oil. *Bioresour. Technol.* **2009**, *100*, 4690–4696. [CrossRef] [PubMed]
35. Yamaguchi, T.; Wang, Y.; Komatsu, M.; Ookawa, M. Preparation of new solid bases derived from supported metal nitrates and carbonates. *Catal. Surv. Jpn.* **2002**, *5*, 81–89. [CrossRef]
36. Genge, M.J.; Jones, A.P.; Price, G.D. An infrared and Raman study of carbonate glasses: Implications for the structure of carbonatite magmas. *Geochim. Cosmochim. Acta* **1995**, *59*, 927–937. [CrossRef]
37. Piriou, B.; Mcmillan, P. The high-frequency vibrational spectra of vitreous and crystalline orthosilicates. *Am. Mineral.* **1983**, *68*, 426–443.
38. Ma, F.; Hanna, M.A. Biodiesel production: A review. *Bioresour. Technol.* **1999**, *70*, 1–15. [CrossRef]
39. Dawodu, F.A.; Ayodele, O.; Xin, J.; Zhang, S.; Yan, D. Effective conversion of non-edible oil with high free fatty acid into biodiesel by sulphonated carbon catalyst. *Appl. Energy* **2014**, *114*, 819–826. [CrossRef]
40. Muthu, H.; SathyaSelvabala, V.; Varathachary, T.; Kirupha Selvaraj, D.; Nandagopal, J.; Subramanian, S. Synthesis of biodiesel from neem oil using sulfated zirconia via tranesterification. *Braz. J. Chem. Eng.* **2010**, *27*, 601–608. [CrossRef]
41. Rashid, U.; Anwar, F.; Knothe, G. Evaluation of biodiesel obtained from cottonseed oil. *Fuel Process. Technol.* **2009**, *90*, 1157–1163. [CrossRef]